SP-268—1

Application and Modeling of Steel Fiber-Reinforced Concrete for Buried Structures

by D. M. Brodowski, M. G. Katona, and J. A. Pope

Synopsis: The current research shows that the addition of steel fibers to plain concrete is effective in enhancing the tensile ductility and loading capacity of buried concrete structures such as bridges, culverts, and vaults. This paper details the development of a steel fiber reinforced concrete (SFRC) analytical model used in the finite element program, CANDE, and describes the experimental and analytical approach used to test the accuracy of the model. The results of full-scale, in-place load tests on many precast buried SFRC arch structures (composed of less than or equal to 1% steel fibers by volume) correlated well with the CANDE model predictions. The CANDE program exhibits the ability to model the material behavior of SFRC as well as the effects of soil-structure interaction. The analytical and experimental research summarized in this paper leads to the ability to design SFRC for structural applications such as buried bridges, culverts, and vaults.

Keywords: arch; bridge; buried structure; culvert; fiber-reinforced concrete (FRC); precast concrete; steel fiber; tensile behavior.

ACI member ***David Brodowski*** is the Senior Bridge Engineer with the Montgomery County Engineer's Office in Dayton, OH. His previous experience as a Product Manager for CONTECH Construction Products Inc. focused on the use of precast concrete buried structures in civil infrastructure. He received his MS in civil engineering at the University of Cincinnati in 2005, with a thesis on developing an appropriate steel fiber-reinforced concrete for applications to buried structures.

Michael G. Katona, PhD, recently retired as Professor and Chair from the Department of Civil and Environmental Engineering at Washington State University. He now serves as a private consultant specializing in numerical analysis techniques applied to soil-structure interaction problems. He is the principal author of the computer programs sponsored by FHWA and AASHTO that are used world wide for the design and analysis of buried culverts and structures.

Jacob A. Pope graduated from the University of Cincinnati in 2004 with a BS in civil engineering. His master's thesis focuses on correlating previous steel fiber concrete research to full-scale load testing and modeling. He currently promotes, designs and supplies precast concrete buried structures for Precast Forum, LLC in Wildwood, MO.

INTRODUCTION

Steel fibers have been widely used as secondary (temperature-shrinkage) reinforcement for many precast, cast-in-place, and shotcrete applications. Popular structural applications that take advantage of the increased flexural strength of steel fiber reinforced concrete include bridge decks, pavements, tunnel and canal linings, hydraulic structures, pipes, and tilt-up panels. The research reported herein focuses on an application of steel fibers to precast buried concrete structures, where the resistance of the structure is provided only by the steel fiber reinforced concrete member and the surrounding soil.

Predicting the performance of a buried structure to take advantage of the improved ductility is difficult since no standard design methodology exists for steel fiber-reinforced concrete (SFRC) and the analysis of the soil-structure interaction is complex. The analysis is dependent upon many variables such as the geometry and stiffness of the structure, properties of the surrounding soil, the loading conditions, the construction operation, the type and volume of steel fiber in the concrete mix, and the mix design itself. The key structural variables are simulated in the design and analysis software Culvert Analysis and Design (CANDE). According to the Transportation Research Board's NCHRP program, CANDE is the "premier design and analysis tool for all types and sizes of buried culverts…and is widely used by state highway departments, industry, consulting firms, and universities in the United States, Canada, Europe, Africa, and Australia" (1). This paper details the analytical model for steel fiber reinforced concrete utilized by the CANDE program.

Previous research was performed to determine the flexural properties of steel fiber mix designs with dosages ranging from 0.66 to 4.00% by volume (2). Using the experimental flexural strength properties of first crack stress and rupture stress for each mix design, CANDE was used to analyze numerous geometries and section thicknesses to design a buried precast arch structure. The final precast arch structure made optimum use of the concrete and steel fiber materials while providing a safe design for highway loading. The optimization considered the economics of the steel fibers, the concrete, and the overall weight of the unit for shipping considerations. The end result was a proposed arch structure with a span of 8.5 feet (2.59 m), a rise of 6.0 feet (1.83 m), and length of 6.0 feet (1.83 m).

This paper will report the theoretical background and assumptions used to model the SFRC structure and the experimental and analytical results of an in-place, full-scale load test. Comparisons of a SFRC arch and plain concrete arch are presented to demonstrate the significantly increased load carrying capacity of the SFRC arch for the same geometry and loading conditions.

RESEARCH SIGNIFICANCE

Although research has shown that the addition of steel fibers to concrete improves the ductility and shear capacity of the concrete, no design procedures or codes exist in the United States for the routine design of SFRC structures. This paper presents an analytical model that correlates well with experimental data that can be used to model and design SFRC members.

ANALYTICAL MODEL PURPOSE

The intent of this section is to present the theoretical assumptions and developments for modeling structural members composed of steel fiber reinforced concrete (SFRC). As a result of the study presented herein, the SFRC model was incorporated into a special version of the CANDE finite element computer program especially for the design and analysis of the precast arch described in this paper.

Background

First introduced in 1976 under the sponsorship of the Federal Highway Administration, CANDE was developed for the structural design, analysis and evaluation of buried structures including culverts made of corrugated metal, reinforced concrete, and plastic as well as other soil-structure interaction problems such as underground storage facilities, storm water runoff chambers, retaining walls, tunnel liners, and protective structures. Over the years FHWA has sponsored several upgrades to the program, and AASHTO is currently sponsoring several additional enhancements to CANDE under NCHRP Project 15-28 (3-6).

CANDE is a two-dimensional, plane-strain finite element program with the following key features:

- Incremental construction – the capability to simulate the physical process of placing and compacting soil layers, one lift at a time, below, along side and above the culvert as the installation is constructed.
- Interface elements – the ability to simulate the frictional sliding, separation and re-bonding of two bodies originally in contact. Typically these elements are used between the culvert and soil and between trench soil and in situ soil.
- Soil elements and models – soil elements are high-order continuum elements with a suite of soil models ranging from linear elastic to highly nonlinear. The so-called Duncan and Duncan/Selig soil models are very representative of the nonlinear soil behavior in most culvert installations.
- Beam elements and pipe models – A culvert (or structure) is represented by a connected sequence of short beam-column elements that trace the culvert's periphery. The material models of beam-elements distinguish between different pipe types. Each material model includes design criteria, which provide measures of safety against potential modes of failure.
- In particular, the reinforced concrete beam element is composed of a plain concrete matrix along with rows of reinforcing steel located at discrete points in the concrete cross section. Concrete behavior is characterized by cracking in tension and plastic hardening in compression. Reinforcing steel behavior is simulated as elastic - perfectly plastic in tension and compression. Design criteria for reinforced concrete culverts include safety factors for steel yielding, ultimate concrete crushing, excessive shear stress, and excessive concrete cracking (crack width estimate). The material model is discussed below.

Plain concrete model

The constitutive model used to simulate the concrete matrix of the reinforced concrete beam element discussed above provides a reference to compare and contrast the new SFRC model presented in this paper. To this end, Figure 1 illustrates the uni-axial stress-strain relationship for a plain concrete specimen that has not been previously loaded.

The plain concrete model in the figure is defined by the following independent parameters:

- e_c = compressive strain at initial ultimate strength of concrete
- e_y = compressive strain at initial plastic yielding of concrete
- e_t = tensile strain when concrete abruptly cracks (stress released)
- E_c = Young's modulus of concrete in elastic zone
- f_c = ultimate compressive stress of concrete

Plain concrete parameters derived from the above independent parameters include:

- $f_t = E_c\, e_t$ = tensile stress when concrete abruptly cracks (stress released)
- $f_y = E_c\, e_y$ = compressive stress at initial plastic yielding of concrete

To better explain the plain concrete model, let the symbol 'e' represent an applied strain loading and the symbol 'f' denote the corresponding stress, therefore df/de is the stress-strain modulus at various regions on the loading/unloading path. With this understanding, the model's compression and tension behavior are discussed in turn:

Compression region:

- Initial compression loading is linear elastic when the applied strain is in the range 0 to e_y, which implies df/de = E_c
- Plastic hardening occurs when the applied strain is in the range e_y to e_c, wherein df/de = $(f_c - f_y)/(e_c - e_y)$ and some plastic strain is accumulated.
- Perfect plasticity occurs when the applied strain exceeds e_c, wherein df/de = 0 and plastic strain is accumulated.
- Upon unloading from anywhere in the compression region (i.e. the applied compressive strain is reduced) the response is elastic, df/de = E_c.
- Tension region:
- Initial tension loading is linear elastic when the applied strain is in the range 0 to e_t wherein df/de = E_c (virgin material only)
- Abrupt concrete cracking occurs when the applied strain exceeds e_t for the first time. All stress is released so that df/de = $-f_t$ and tensile-strain-damage begins to accumulate. For all future load-paths, the concrete is assumed non-healing so that f_t and e_t = 0 for all time, (meaning the tension triangle in the virgin stress-strain curve has become a flat line).
- Continuing the applied tensile strain beyond the initial cracking strain results in further accumulation of tensile-strain-damage while the stress remains zero, df/de = 0.
- Upon unloading from anywhere in the tension region after tension damage has occurred produces no change in stress (df/de = 0) until the unloading strain overcomes the accumulated damage strain (i.e., closing of smeared cracks).

The plain concrete model has performed well and has been operative in CANDE since 1980 (7). As a preview to the SFRC model development in the next section, we note that the behavior of plain concrete and fiber-reinforced concrete are very similar in compression. For tension however, fiber-reinforced concrete exhibits much more ductility than does plain concrete.

SFRC model

Existing experimental knowledge as well as experimental knowledge gained during the course of this study was used to guide the development of the SFRC model (2, 8). These experiments included various types and lengths of steel fibers added into the concrete mix at volume percentage ranging from 0 to 4% and tested in uniaxial compression, tension, and in beam bending.

Although the tests exhibited some variability, two key observations appear generally valid:

- The addition of steel fibers has negligible influence on compressive strength or the character of the compressive stress-strain relationships.
- The addition of steel fibers has very little influence on tensile strength, that is, f_t remains practically unchanged. However, the tension ductility is significantly increased as the percent of steel fibers is increased.

The increase in tensile ductility means that rather than an abrupt loss of stress after the concrete cracks, the stress reduces more gradually because the fibers spanning the crack allow some tensile stress to remain, which decreases gradually to zero as tensile strain increases causing more fibers to break or lose anchorage in the concrete.

Based on the these two key observations, a simple alteration to the plain concrete stress-strain model was devised to simulate the behavior of fiber reinforced concrete as illustrated in Figure 2. In this model the steel fibers and concrete are viewed as a mixture, not separate materials.

The SFRC model includes one additional independent parameter beyond that of the plain concrete model, which is called the tensile rupture stain denoted as e_r. The parameters in the compression region remain as defined for plain concrete whereas the tension parameters are redefined as follows:

- e_t = tensile cracking strain indicating the initial cracking of concrete (typically the same value as plain concrete)
- e_r = tensile rupture strain indicating the tensile strain level at which all stress is released (inferring that all steel fibers spanning the gap have broken or have lost anchorage)
- SFRC model parameters derived from the above independent parameters are defined as:
- $r = e_r / e_t$ = ratio of rupture strain to initial cracking strain, $1 \le r \le \infty$. Note that for the limiting value r =1, the SFRC model is identical to the plain concrete model.

- $f_t = E_c e_t$ = tensile stress when concrete initially cracks (typically the same value as plain concrete).
- $E_s = -f_t/(e_r - e_t)$ = negative modulus of concrete in the softening zone.

In the compression region the rules governing the SFRC model are identical to the rules discussed above for plain concrete. In the tension region the rules governing the SFRC model are summarized below where df/de is the stress-strain modulus at various regions on the loading/unloading path. The symbol f is the stress associated with the applied strain e.

Tension region:

- Initial tension loading is linear elastic when the applied strain is in the range 0 to e_t wherein df/de = E_c (virgin material only)
- Concrete cracking begins when the applied strain, e, exceeds initial cracking strain, e_t, for the first time. Tension damage strain, defined as $e-e_t$, is accumulated during this process. For the case when the applied strain is in the range, $e_t \le e \le e_r$, the stress loss is $\Delta f = E_s(e - e_t)$ so that the current stress is given by $f = f_t - \Delta f$. When damage occurs, the virgin stress-strain curve is redefined by assuming a straight line between the origin and the current stress/strain point. Said another way, the left side of the tension triangle becomes flatter and flatter with the triangle apex located at the stress-strain point (f,e).
- Continuing the applied tensile strain beyond the rupture strain results in further accumulation of tension damage strain and a complete loss of stress, $\Delta f = f_t$ so that f = 0. Thus the initial tensile triangle of the virgin stress-strain curve becomes a flat line wherein df/de = 0.
- Upon unloading from the tension region after partial tension damage has occurred, the unloading modulus df/de is the current slope of the left triangle leg, representing a small positive stiffness of the remaining steel fibers that are being relieved of tension.
- Upon unloading from the tension region after complete tension damage has occurred there is no change in stress (df/de = 0) until the unloading strain overcomes the accumulated damage strain (that is, closing of smeared cracks).

Load capacity of SFRC model

When comparing the stress-strain figures of the plain concrete model and the SFRC model, it may appear that the load capacities of the two models are the same. Indeed, this observation is true for a test specimen loaded in pure axial tension wherein the ultimate tensile load for both models is easily computed as $T = f_t A$ where A is the cross-sectional area of the test specimen.

However for a test specimen loaded in pure bending, it is quite remarkable that the ultimate moment capacity of the SFRC model is appreciably greater than the plain concrete model depending of the value of the parameter r, (the ratio of rupture strain to initial cracking strain). Because this statement may not be intuitively obvious, a derivation of moment capacity is provided in the following development.

Consider a beam specimen in pure bending with a rectangular cross-section of height h and width b. Assuming planes remain plane for all load levels, the strain profile is linear through the height of the cross section. Thus, the strain profile e(y) is completely defined by two points for which we choose the bottom fiber and the neutral axis. At the bottom fiber the strain is prescribed as $e(0) = e^*$ where e^* is characterized by an x-multiplier of the initial cracking strain ($e^* = x e_t$). By definition the strain at the neutral axis is zero, $e(y^*) = 0$, where y^* is characterized by a z-multiplier of the cross-section height ($y^* = zh$). Figure 3 illustrates these basic assumptions.

The location of the neutral axis y^* (z-multiplier) is dependent on the stress profile which in turn is dependent on the magnitude of the prescribed strain e^* (x-multiplier). Because the tensile portion of the SFRC stress-strain relation is defined by three piecewise linear regions, we develop the stress profile for three ranges of the e^*:

1. Maximum tensile strain e^* is in the uncracked virgin range, $0 \le x \le 1$
2. Maximum tensile strain e^* is in the softening range, $1 \le x \le r$
3. Maximum tensile strain e^* exceeds the rupture strain, $r \le x \le \infty$

The corresponding stress profiles for these three regions are illustrated in Figure 4 wherein it is reasonably assumed that maximum compressive stress in the top fiber remains within the elastic range.

Since the stress profiles are a result of pure bending, the neutral axis (z-multiplier) is determined by requiring the sum of the forces equal zero. After determining the location of the neutral axis, the internal moment can be computed by integration. Table 1 summarizes the results, where $M_t = f_t bh^2/6$ is the moment that causes initial tensile cracking on the bottom fiber when x = 1 and is the maximum moment capacity for the case r =1 (plain concrete).

Except for the linear range, the equations for the internal moment do not lend themselves to easy interpretation without graphical aid. Figure 5 shows plots of the non-dimensional moment, $m(x) = M(x)/M_t$, for a family of ratios, r = 2, 5, 10, and 20. All families trace the same straight line in the linear range $0 \le x \le 1$, then diverge into separate bell-shaped curves in the softening range $1 \le x \le r$, and asymptotically approach zero in the rupture range $r \le x \le \infty$. It is evident that the peak moment (maximum moment capacity) occurs in the softening range and increases with the r-ratio. For r = 20, it is observed that the moment capacity is 1.8 times that of plain concrete.

From Table 2 we see that fiber reinforced concrete with an r-value on the order of 100 more than doubles the moment capacity of un-reinforced plain concrete. This finding provides the impetus to continue the model development for real-world applications.

CANDE finite element development

The last portion of the overall analytical development is to incorporate the SFRC constitutive model into a beam-column element and outline an overall solution strategy. The nonlinear solution strategy is well documented in other publications (2, 4, 7) and is outlined below.

The overall finite element methodology is based on a displacement-formulation of virtual work with the following assumptions:

- Incremental load steps, i = 1 to N
- Bernoulli-Euler beam theory with axial deformation
- Hermetian interpolation functions for transverse bending displacements
- Linear interpolation functions for axial displacements.

This methodology results in a beam element stiffness matrix, $\underline{K}$, which relates increments of displacement to increments of load, from step i-1 to i. The element stiffness matrix can be written in the standard form as a combination of bending stiffness geometry $\underline{K}_b$ and axial stiffness geometry $\underline{K}_a$ as,

$$\underline{K} = (E_c I^*)\,\underline{K}_b + (E_c A^*)\,\underline{K}_a$$

A* and I* are called effective section properties, which, along with the neutral axis y*, are dependent on the nonlinear stress-strain model and are calculated by integration over beam cross section:

1. Effective area: $A^* = (1/E_c)\int_A E^*(y)dA$
2. Neutral axis: $y^* = (1/E_c)(\int_A yE^*(y)dA)/A^*$
3. Moment inertia: $I^* = (1/E_c)\int_A (y-y^*)^2E^*(y)dA$

E*(y) is the current chord modulus at position y that connects the SFRC model stress-strain point at step i-1 to the stress-strain point at step i. If E*(y) is in the linear range for all y, then $E^*(y) = E_c$, and the above integrals may be integrated exactly to produce the familiar cross section properties for linear elastic beams.

In general, however, the integrals must be calculated numerically. CANDE employs 11-point Simpson integration through the beam depth. History information is retained at each of the 11 integration points, which includes the total stress and strain value after the last converged load step along with updated damage and plasticity parameters that define the current shape of the SRFC stress-strain curve.

To advance from load step i-1 to i, the values for A*, y* and I* are determined iteratively because they are dependent on the initially unknown values of E*(y). The solution is iterated until successive iterations produce values A*, y* and I* that converge within 0.1% error. During the iteration process the chord modulus is recomputed at each integration point as $E^*(y) = (f_i - f_{i-1})/(e_i - e_{i-1})$, where f_{i-1}, e_{i-1} are the known stress and strain values for load step i-1, e_i is the current iterative prediction for strain at load step i, and f_i is determined from the SFRC model based on the current strain estimate e_i.

The overall solution strategy is summarized in Figure 6, which concludes the presentation on the analytical development.

EXPERIMENTAL PROGRAM

Full-scale test specimens

The arch-shape for the full-scale load test had a span equal to 8.5 feet (2.59 m) a rise of 6.0 feet (1.83 m) and length of 6.0 feet (1.83 m). Five arch units were tested. The arch thickness varied from 4.5 inches (114 mm) at the crown of the arch to 3.0 inches (76 mm) thickness at the base of the arch leg for units 2, 3, and 4, and 4.0 inches (102 mm) to 2.5 inches (64 mm), respectively, for units 1 and 5. The mix design and resulting compressive strength of each arch unit tested is shown in Table 3. Unit 1 was plain concrete, while units 2-5 were fiber reinforced with the dosages shown in Table 3. Unit 3 consisted of hooked end steel fibers with a diameter of 0.035 inches (0.90 mm) and length equal to 2.36 inches (60 mm). Units 2, 4 and 5 consisted of twisted steel fibers with a diameter of 0.02 inches (0.50 mm) and length equal to 1 inch (25 mm). Steel fibers conformed to ASTM A820. Fibers were added to the concrete directly in the ready mix truck. Because of the self consolidating mix, no external vibration was used when placing the concrete into the form. The units were poured on their sides as shown in Fig. 7, and cured under field conditions.

Test setup

A structural base slab supported the arch units and was designed to resist the jacking forces during the load test. Four units were placed on the base slab at a time. The two inner units were tested in sequence, while the two outer units were in place to retain the backfill. From preliminary CANDE analyses, the arch units experienced the greatest tensile stresses when loaded with live loads under minimal earth fill heights. Therefore, the units were covered with 1 foot (305 mm) of fill over the crown of the arch (a typical industry standard for minimum earth cover).

Backfilling the arch units was strictly monitored to assure the installation was properly constructed. An AASHTO A1 material was used and compacted to 90% standard proctor. The backfill was placed in 6 inch (153 mm) lifts on each side of the arch unit and tamped with a plate compactor. A geotechnical consultant verified that each lift was compacted to 90% standard proctor after each lift.

The arch units had a 4 inch (102 mm) diameter hole cored in the crown through which a dywidag bar was placed (see Figure 8). The dywidag bar attached to a coupler cast into the foundation extended upward through the arch unit, earth fill, loading block and through the center of a 100-ton (890 kN) hydraulic jack. A large nut was twisted down the dywidag bar until it came in contact with the top the hydraulic jack. Below the hydraulic jack was a load cell that was calibrated to measure the load during testing. A strain gage on the load cell was connected to the data acquisition center on site which provided real time read outs of the load that was recorded for later analysis. The load from the jack was transferred to the soil through a loading block created out of two layers of intersecting wide flange steel beams (see Figure 9). The beams rested on top of two 0.25 inch (6 mm) thick plywood distribution plates. The distribution plates measured 3.0 feet (915 mm) by 3.0 feet (915 mm). These plates transferred the load to the soil.

The arch unit's displacements during loading were measured by DCDT transducers placed inside the arch prior to testing. A total of eight transducers where used on each arch unit being tested. Transducers were placed symmetrically about the load and anchored at the bottom of the arch unit legs, next to the foundation. There were four transducer stations on each arch unit while being tested. Each station held two transducers in place, as shown in Figure 10. The stations were placed symmetrically about the load and at the inside bottom of the arch unit leg where it met the foundation. At each station, one transducer was stretched to the top of the inside arch and the other transducer was stretched to a spot that was on the opposite leg and halfway up the arch. The transducers connected to the top of the arch were in place to measure mid-span deflection and the others were in place to measure any possible racking. Stations were placed across from each other on opposite legs. Four stations where used on each arch unit, two on each side of the dywidag bar. This positioning of stations allowed for monitoring any inconsistencies along the length of the arch unit such as fiber distribution, uneven loading, or racking. The transducers were connected by a wire to the data acquisition center on site.

Test procedure

The arch units were loaded one at a time. The jack was slowly opened to increase the pressure applied to the distribution plate and the soil on top of the arch unit. The data acquisition center recorded the load and corresponding displacements. Team members were stationed below the unloaded arch units to record the load at the first visible crack and to observe the cracking pattern. The jack was continuously opened until the load on the arch unit started to drop off. After testing, the load block, jack and transducers were moved to the adjacent arch unit for the next test. As a result of the low earth fill, the load being centered on the arch unit, and the lack of shear connectors between units, no load was transferred from one unit to the next during testing. The duration of each test varied from 10 minutes minimum to 20 minutes maximum.

TEST RESULTS AND ANALYSIS

The DCDT transducers measured the change in the length of the cord that was attached to it. The rise of the arch unit, half the span length and the wire attached to the DCDT formed a right triangle, which permitted triangulating and measuring the mid-span deflection during testing.

Figure 11 shows the load vs. deflection results for the five arch units tested. The deflections are reported at mid-span of the arch, the location of maximum vertical displacement. It can be seen that the fiber reinforced units (units 2-5) sustained a peak load ranging from 117 kips (520 kN) up to a maximum of 152 kips (676 kN), dependent on the percentage of steel fibers. The plain concrete arch, unit 1, only sustained a peak load of 100 kips (445 kN). The contribution of the fibers in the concrete is most evident post crack. As shown in Figure 11, the fiber reinforced units carried an average load nearly 1.5 times the load carried by the plain concrete unit for the same deflection up to 0.20 inches (5 mm) of mid-span vertical deflection.

Initial concrete cracking was observed to occur when the load reached about 60 kips (267 kN). This observation is reflected in the initial softening of the load vs. deflection curves at 60 kips (267 kN) for all units. Each test was stopped once the load was unable to be increased with increasing deflection. The units all developed a failure mechanism composed of three cracks along the length of the unit due to tensile stresses. The peak load occurred when the cracks developed into complete hinges. The three hinges were located at the inside face of the arch crown (centerline of arch) and on the outside face of the arch haunches. The two haunch cracks on the outside face were symmetrically located approximately 5.42 feet (1.65 m) from the bottom of the unit (measured vertically, perpendicular to the top of the foundation slab).

Figure 12 shows the experimental results of unit 5 compared to the analytical results obtained from modeling the structure with the CANDE program. CANDE's finite element model includes the structure and surrounding soil along with a series of surface pressure increments to simulate the jacking load. The load vs. deflection curve from CANDE correlates well with the experimental results for initial, linear elastic loading, to nonlinear loading (post-crack behavior), and up to peak load. Peak load prediction by CANDE was within 3% of the measure peak of 152 kips (676 kN). Post-peak loading, or load-softening, was not simulated because the CANDE model was restricted to force-increment loading, not displacement increment loading.

The CANDE model prediction for initial cracking occurred when the load reached about 40 kips (178 kN). Although this load level is less than the experimentally observed first crack at a load of 60 kips (267 kN), the correlation between experiment and prediction is very reasonable in view of the fact that CANDE reported a crack width equal to 0.00096 inches (0.02 mm) at 40 kips (178 kN), which is not likely visible to the naked eye.

With regard to the failure prediction, the CANDE model predicted the same 3-crack hinging failure as observed in the experiment, at the arch crown and arch haunches. Further, CANDE predicted that the inside face of the crown (positive moment region) cracked prior to the outside face of the arch at the haunches (negative moment region). Although the sequence of the cracking could not be physically observed on the outside of the arch because of the soil backfill, the predicted sequence of events correlate well with nonlinear behavior of the load-deformation plot of unit 5 in Figure 11. That is, CANDE predicts the hinge-like cracking at the haunches to start at a load level of 110 kips (489 kN), which correlates well with the start of the slope reduction in the load-deformation plot. The CANDE model predicted the location of the controlling negative moment crack to be at 5.0 feet (1.52 m) from the arch bottom, which is only 5 inches (127 mm) from the experimentally observed location.

In summary, from elastic response to initial concrete cracking to ultimate failure, the CANDE model correlated very well with experimental observations and measurements.

CONCLUSIONS

The current research shows that the addition of steel fibers to plain concrete is effective in enhancing the tensile ductility and loading capacity of buried concrete structures such as bridges, culverts and vaults. This paper explored a practical application of steel fiber reinforced concrete (SFRC) to buried structures, detailed the development of a SFRC analytical model used in the finite element program - CANDE, and described the experimental and analytical approach used to test the accuracy of the model.

The accuracy of the CANDE program, as measured by correlating the results from the analytical model and experimental results of the full-scale load test, suggests that the SFRC model presented is well suited for analyzing and designing SFRC structures. This type of analysis, where the ductility of the material is considered, leads to the ability to investigate structural applications that can take advantage of the additional moment capacity offered by SFRC compared to plain concrete. The methodology presented provides a means to define ductility related to moment capacity, which is the essential link for structural design and the development of new applications for SFRC.

For the application of SFRC to buried structures, the ductility offered by SFRC allows for an appropriately designed structure to take advantage of soil-structure interaction, creating an efficient and economical structure. Since it was shown that the maximum load on the structure was more than two times the required design (factored) load from AASHTO Standard Specifications for Highway Bridges, the thinner of the two arch unit sections tested was considered the most economical section to develop into a new precast product. The product was introduced to the construction market as a solution for small span culverts and stormwater detention vaults. The product is a cost effective alternative to cast-in-place box culverts, corrugated metal pipe, and plastic detention vaults. Currently, there are a number of projects throughout the United States where this product is being utilized as a precast concrete solution for these types of applications. These products have shown economies related to manufacturing, shipping, and installation due to the fact that no conventional reinforcing needs to be tied or placed, multiple units can be placed on a single truck, and only lightweight equipment is needed on site to install the arch units.

ACKNOWLEDGMENTS

Authors would like to acknowledge Dr. Bahram M. Shahrooz, P.E., F.A.C.I. of the University of Cincinnati, Ahern Construction, Moraine Materials, and Miller Valentine Group. We would also like to gratefully acknowledge the support and leadership of Mr. William Lockwood, P.E., Tim Beach, P.E., Mike Carfagno, P.E., and Lynne Vaia, P.E. of CONTECH Construction Products Incorporated.

REFERENCES

1. A2C06 Committee on Hydraulic Structures, Group 2, "Design and Construction of Transportation Facilities," Committee Research Problem Statements, Section C—Structures, Transportation Research Board, http://gulliver.trb.org/publications/problems/A2C06-02.pdf. (accessed 12/16/02)
2. Brodowski, D., "Application of Steel Fiber Reinforced Concrete to Buried Structures," masters thesis, Department of Civil Engineering, University of Cincinnati, Cincinnati, OH, 2005.
3. Katona, M. G.; Smith, J .M.; Odello, R. S.; and Allgood, J. R., "CANDE: A Modern Approach for the Structural Design and Analysis of Buried Culverts," *Federal Highway Administration Report No.* FHWA-RD-77-5, Oct. 1976.
4. Katona, M. G.; Vittes, P. D.; Lee, C. H.; and Ho, H. T., "CANDE-1980: Box Culverts and Soil Models, Federal Highway Administration," *Report No.* FHWA-RD-172, May 1981.
5. Musser, S. C.; Katona, M. G.; and Selig, E. T., "CANDE-89: Culvert Analysis and Design Computer Program User Manual," *Federal Highway Administration Report No.* FHWA-RD-89-169, June 1989.
6. Mlynarski, M.; Katona, M. G.; and McGrath, T. J., "Modernize and Upgrade CANDE for Analysis and Design of Buried Structures," *Interim Report for AASHTO NCHRP* 15-28, Nov. 2005.
7. Katona, M. G., and Vittes, P. D., "Soil-Structure Evaluation of Buried Box Culvert Designs," *Transportation Research Record*, No. 878, 1982, pp. 1-7.
8. ACI Committee 544, "Design Considerations for Steel Fiber Reinforced Concrete (ACI 544.4R-88)," American Concrete Institute, Farmington Hills, MI, 1999.

Table 1—Neutral axis location and internal moment values as a function of x and r

Range of x-multiplier ($e^* = xe_t$)	Neutral axis location ($y^* = zh$)	Internal Moment ($M_t = f_t bh^2/6$)
Linear range $0 \le x \le 1$	$z = ½$	$M(x) = M_t\, x$
Softening range $1 \le x \le r$	$z(x) = ((1+a)^{1/2} - 1)/a$ where, $a = (x-r)/(r-1)/x^2 - 1 + (2r-x-1)/(r-1)/x$	$M(x) = M_t[2(1-z)^3 x/z + z^2(3r-2x-r/x^2)/(r-1)]$
Rupture range $r \le x \le \infty$	$z(x) = 1/(1 + r^{1/2}/x)$	$M_t[2x(1-z)^3/z + z^2(r^2+r)/x^2]$

Table 2—Moment capacity factor versus increased values of r by powers of 10

r-value	1	10	100	1000	10,000
M_{max}/M_t	1.0	1.6	2.2	2.6	2.8

Table 3—Material properties of the precast arch units

	Mix Proportions per 1 yd^3, SSD Condition							14-day	28-day
	Gravel 8's	Sand	Cement	Water	Superplasticizer	Visc. Modifier	*Steel Fibers	f'c	f'c
	(lbs.)	(lbs.)	(lbs.)	(lbs.)	(oz.)	(oz.)	(lbs.)	psi	psi
UNIT I.D.									
1	1360	1570	702.5	425	84	14	0	7918	9535
2	1400	1540	697.5	409	98	14	100	6111	6575
3	1370	1590	705	392	112	21	135	5148	5485
4	1370	1550	717.5	392	126	21	80	6417	6883
5	1370	1570	710	392	84	14	80	6995	7783
	*Hooked end fibers used for Unit 3, Twisted fibers used for Units 2, 4, & 5								
	1 yd3 = 0.76 m3; 1 lb = 0.45 kg; 1 oz = 30 cm3; 1000 psi = 7 Mpa								

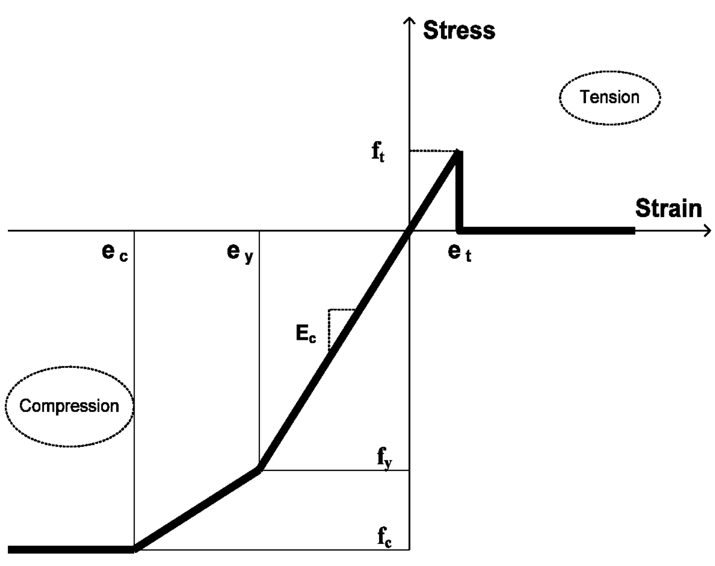

Fig. 1—Plain concrete stress-strain model (virgin curve).